Asian Journal of Chemistry; Vol. 32, No. 4 (2020), 810-814

ASIAN JOURNAL OF CHEMISTRY

https://doi.org/10.14233/ajchem.2020.22460

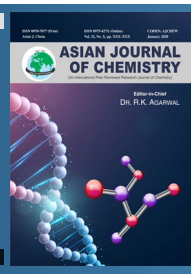

Template-Free Synthesis of Porous Carbon from Merbau Wood by H_2O_2-$ZnCl_2$ Hydrothermal Treatment

DARMA SANTI[1,2,*], TRIYONO[2,*], WEGA TRISUNARYANTI[2] and IIP IZUL FALAH[2]

[1]Department of Chemistry, Faculty of Mathematics and Natural Sciences, Universitas Papua, Manokwari 98314, Indonesia
[2]Department of Chemistry, Faculty of Mathematics and Natural Sciences, Universitas Gadjah Mada, Yogyakarta 55283, Indonesia

*Corresponding authors: E-mail: d.santi@unipa.ac.id; triyn102@ugm.ac.id

Received: 20 September 2019; *Accepted*: 15 November 2019; *Published online*: 25 February 2020; AJC-19796

Zinc(II) chloride, as an activating agent and H_2O_2 as an oxidizing agent, prepared the hydrothermal treatment synthesis of porous carbon (HC). The hydrothermal followed by carbonization and then by oxidation at 350 °C under oxygen stream (HC-Ox). All the products characterized by XRD, FT-IR, amount of oxygenated functional groups (OFGs) obtained by the Boehm method, the total acid amount by NH_3 base vapour adsorption, surface area analyzer (SAA) and SEM. The XRD results showed that all of the carbonized samples were amorphous, which characteristic for porous carbonized. The results of FT-IR and Boehm titration revealed that the phenolic group was the highest contributor to OFGs on HC-Ox samples (7.095 meq/g) and carboxylic groups of 2.685 meq/g. The maximum BET surface area was found to be 443.5 (m^2/g) for C-Ox and 232.2 (m^2/g) for HC-Ox. The SEM image displayed that the morphology of the HC samples was a stacking honeycomb-like structure.

Keywords: Carbon, Hydrothermal, Merbau, Oxygenated functional groups.

INTRODUCTION

In recent times, research activity still needed concerning the development and study of carbon-based materials. These are due to the development of new fields of science and engineering required carbon materials with improved properties, not only include synthesis of allotropic carbons form but also, the development of a wide range of porous materials in the series of mixed carbon forms [1]. Physical activation was the primary method for preparing activated carbons. However, it generally produces microporous activated carbon [2]. Moreover, mesoporous material preparation generally requires a template at high temperatures [3-5]. Besides this method, the synthesis of porous carbon materials developed by the chemical activation methods [6].

On the commercial scale, zinc chloride activation implemented as one of the chemical activation [1], was based on the dehydrating power to eases the breakage of glycosidic linkages. Zinc(II) chloride eliminates hydrogen and oxygen atoms from water present in carbon materials, but not from organic oxygen compounds, which not only leads to the forma-tion of pores and increase in carbon content [7] but also increase in oxygenated functional groups (OFGs). The high surface area mesoporous activated carbons resulted from the use of hydrogen peroxide after zinc chloride activation *via* successively hydrothermal [8]. The presence of high OFGs content on the surface due to zinc chloride activation makes it more suitable for H_2O_2 activation. Hydrogen peroxide as an oxidative agent in this work was predicted to increase the affinity $ZnCl_2$ as an agent of activating on the precursor surface so that improving to higher volume and mesopore area.

In previous studies [9], Merbau wood having potential as carbon precursors, due to the sawdust containing, hemicellulose and lignin [10]. Dependency between OFG in the precursor as the functional property of the starting materials and mesopore area in carbon, which are suitable as surface characteristics of carbon. This work evaluated the preparation of carbon materials using zinc chloride as a chemical agent and hydrogen peroxide as an oxidative agent *via* hydrothermal and continued with physico-chemical activation using the flow of oxygen gas in a furnace.

EXPERIMENTAL

The carbon materials of Merbau wood samples were obtained from Manokwari, Indonesia. The chips of merbau wood were first dried at 110 °C. Prior to any carbonization and oxidization processes, hydrothermal treatment was carried out to promote the chemical activation of samples. Carbonization and oxidization were carried out in a vertical stainless steel reactor of length 50 cm an internal diameter of 30 cm. $ZnCl_2$, H_2O_2 (30 %), NaOH, $NaHCO_3$, Na_2CO_3 and HCl were analytical grade from Merck.

Preparation hydrothermal treatment: The Merbau chips were dried at 105 °C for 24 h and then crushed using a commercial blender to obtain the size of samples of 3-5 mm. A mixture of Merbau chips and H_2O_2 [5.4 g wood chip in 37.5 mL H_2O_2 (10 % by weight)] as the treatment by hydrothermal in an autoclave at 150 °C for 20 min. After the reactor temperature reaches room temperature, the products were dried at 105 °C for 12 h. This product was then mixed with 37.5 mL water and 11.25 g $ZnCl_2$ and then were treated in the autoclave at 200 °C for 20 min. After the reactor was cool, the products were dried at 105 °C for 12 h.

Carbonization and oxidation: The dried samples (resulted from hydrothermal treatment and non-hydrothermal/dried precursors) were loaded on a stainless tube, which was placed inside a tubular stainless reactor in the furnace. The carbonization temperature of 700 °C under of N_2 gas at a flow rate of 20 mL/min for 2 h, at a rate of 10 °C/min. The furnace was cooled to room temperature under nitrogen gas with a constant flow rate. After that, the carbonized samples were prepared into a reactor as used as carbonization steps, with a temperature of the oxidation process of 350 °C at the oxygen stream at a flow rate of 15 mL/min. After the furnace was cooled to room temperature, the activated carbonized were loaded into the desiccator. The product resulted from hydrothermal treatment, before the oxidation steps, was abbreviated as HC and the product resulted from non-hydrothermal/raw dried samples and after the oxidation was noted as C. The HC produced after oxidation step was abbreviated as HC-Ox and C samples resulted after oxidation was noted as C-Ox.

Characterization of carbonized samples: The decomposition rate and temperature range of Merbau wood as raw materials determined by thermogravimetric. This has been achieved using a DTG60 in which 2.889 mg of sample, start temperature at 30 °C up to 600 °C, at a rate of 10 °C/min. DSC60 Plus in which 4.100 mg of sample was treated under nitrogen flow at 30 mL/min.

X-ray diffractogram (XRD) of the synthesized materials was recorded using a Rigaku Miniflex600, λ = 1.54 Å, 40 kV, 15 mA). Adsorption isotherm, BET surface area (S_{BET}) and pore volume of the carbonized samples were obtained by using gas sorption analyzer (SAA, Quantachrome NovaWin Series). Prior to nitrogen adsorption-desorption studies, the samples were degassed at 300 °C for 3 h.

Boehm titration was applied to investigate acidic sites on the surface of porous carbons. Refer to the modified method [11], the samples mixed with three reaction bases of 0.05 M $NaHCO_3$, Na_2CO_3 and NaOH. The suspensions were agitated by a magnetic stirrer for 24 h at room temperature, filtered and 10 mL of the filtrate was pipetted and titrated with 0.05 M HCl to calculate the amount of acidic site [12-14]. The qualitative analysis of test acidity based on Boehm titration of (OFGs) and based on adsorption vapour base of ammonia carried out by the FT-IR spectroscopy.

The texture of the carbonized samples were investigated by scanning electron microscopy (SEM, Jeoul JSM-6510). The samples were prepared by attaching carbonized Merbau woods to carbon tape, with a sputter-coated platinum layer on the sample surface at 15 kV accelerating voltage.

RESULTS AND DISCUSSION

TGA/DTA curves of merbau woods: It's well known that materials lignocellulose, such as Merbau woods, usually consists of lignin, cellulose and hemicellulose. The decomposition of hemicellulose and cellulose under slow pyrolysis begins at 250 °C with the maximal of mass loss at 400 °C [15]. Others reported that the decomposition of lignin, cellulose and hemicellulose take place at ranges of 300-400, 180-240 and 230-310 °C, respectively [16]. Lignin begins decomposing at low temperatures (160-170 °C) and continues to decompose at a low rate until approximately 900 °C. After that, followed by cellulose, in a narrow temperature interval from about 200 to 400 °C. Fig. 1 showed the TGA and DTA curves of Merbau wood as raw materials. It was shown that the carbonization process took in three stages. The first stage attributed to dehydration occurred at a temperature range 30-170 °C. The weight loss was only 9.21 %, it could be ascribed to the elimination of water (such as free water and bound water) and light volatile materials [17]. The second stage takes place at a temperature range of 170-380 °C, which could be associated with the decomposition of hemicellulose and weight loss was 46.63 %. The pyrolysis of cellulose and lignin occurred at 380-521 °C, which consist of 44.65 % weight loss. TGA/DTA curves tend to flatten due to the decomposition of lignin at a higher temperature. The results were in accordance with previous reports [18,19]. However, it is believed that the decomposition of lignin caused the long flat tail observed at high temperatures. It is well known that the unstable volatiles on the carbon samples was decreased when the carbonization temperatures increase. Consequently, the weight losses of Merbau wood during 500-600 °C were larger than those of over 600 °C. These findings are consistent with the lignin was more preferable to the carbons formation than cellulose and hemicellulose [18].

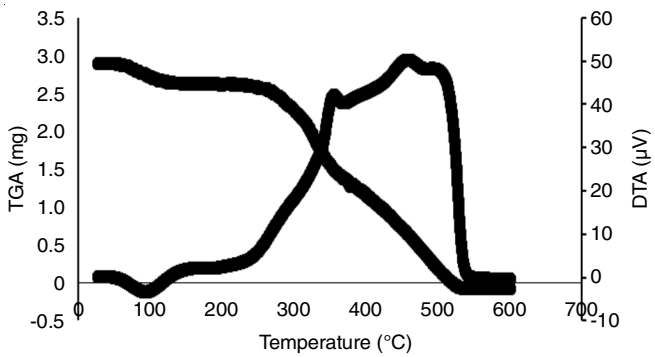

Fig. 1. TGA/DTA curves of Merbau woods

XRD analysis: The XRD patterns (Fig. 2) showed that the structure was changed due to the carbonization and hydrothermal process. The raw diffractogram was showed three peaks that similar to those reported by Jain *et al.* [20]. This pattern was in agreement with the microcrystalline cellulose XRD pattern with amorphous carbon. The all of carbonized and oxidized of C sample patterns were showed two broad peaks that have centered at 2θ = 23° and 43°. These peaks indicated randomly oriented graphitic layers in the material that correlated with amorphous carbon, correspond to (002) and (101) reflection planes in turbostratic carbon structure [21,22].

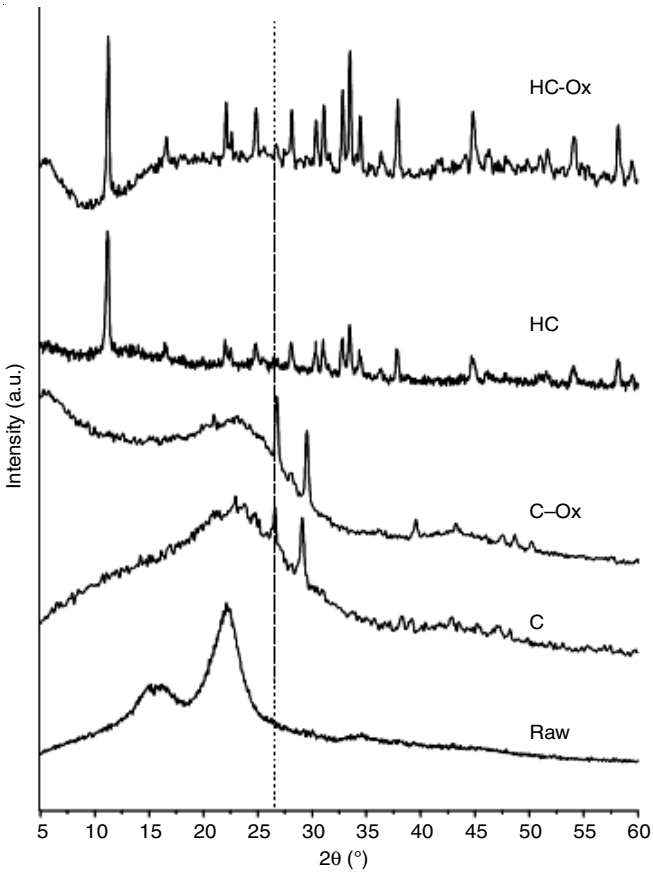

Fig. 2. XRD patterns of raw of Merbau woods, C, C-Ox, HC and HC-Ox

The hydrothermal treatment of HC samples affected the structure of carbonized samples as shown in Fig. 2. The two broad peaks that exhibited in C and C-Ox samples patterns were not seen at HC and HC-Ox patterns. It could be explained by the effect the $ZnCl_2$ and H_2O_2 that would defect of the structure of cellulose, it is clearly shown by decreasing the intensity of microcrystalline cellulose peaks. The glycosidic linkages were easily broken by $ZnCl_2$, however, H_2O_2 as an oxidating agent would convert the cellulose to oxy-cellulose which might also caused by the formation of carboxylic groups [23].

Analysis of OFGs by Boehm titration methods: Fig. 3 showed the number of OFGs on the carbonized samples non-hydrothermal treatment (C-Ox) and hydrothermal treatment (HC-Ox). The OFGs content increased due to effect $ZnCl_2$ as an activating agent and H_2O_2 as an oxidating agent on the precursor surface. The coordinated water molecules act as nucleophiles and Zn^{2+} as shells of hydration in solution [24].

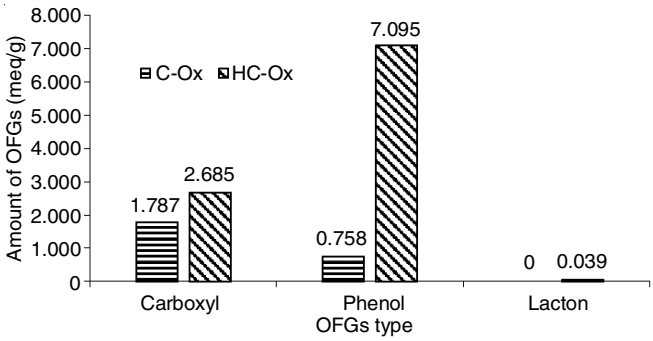

Fig. 3. Acidic groups of C-Ox and HC-Ox samples based on Boehm titration method

These nucleophiles were attracted to the free electron pairs of the oxygen atoms in the OFGs, therefore the greater access for Zn^{2+} to the surface of a precursor which supports the better lignocellulosic biomass dehydration [8]. This advantage was improved by the existence of H_2O_2 to induce the formation of OFGs on the precursor. Carboxylic, lactonic and phenolic groups were obtained on the carbonized surface samples.

Acidity test based on ammonia vapour adsorption and FT-IR analysis: The FT-IR spectra of the carbonized samples are shown in Fig. 4. The main surface OFGs suggested as hydroxyl and carboxylic groups. The FT-IR spectra of all these displayed the following bands: 3495, 3487, 3448, 3425 cm^{-1} corresponding to OH bond stretch. Vibration between 3000 and 2810 cm^{-1} was related to CH stretching. Spectrum for oxygenated carbonized samples shows a low-intensity band in this region. The samples showed bands at 1581, 1573, 1512, 1604 and 1620 cm^{-1} corresponded to aromatic C=C stretching and the C-H deformation of CH_3 [12]. The oxidation and adsorption NH_3 process showed an increasing intensity band of both hydrothermal and non-hydrothermal treatment of samples. The FT-IR spectra of non-hydrothermal samples showed the band of 1442 and 1435 cm^{-1} may be related to OH-groups of carboxylic acids and phenols [25]. After the adsorption of NH_3, there was a new band at 1388 cm^{-1} and a broad absorption band at 3394 cm^{-1} of hydrothermal treatment samples. The band at 3394 cm^{-1} may be attributed to the overtones of N-H and O-H stretching vibrations [12]. The band at 1388 cm^{-1} is closed to the vibration frequency of NH_4^+ chemically adsorbed on Brønsted acid sites

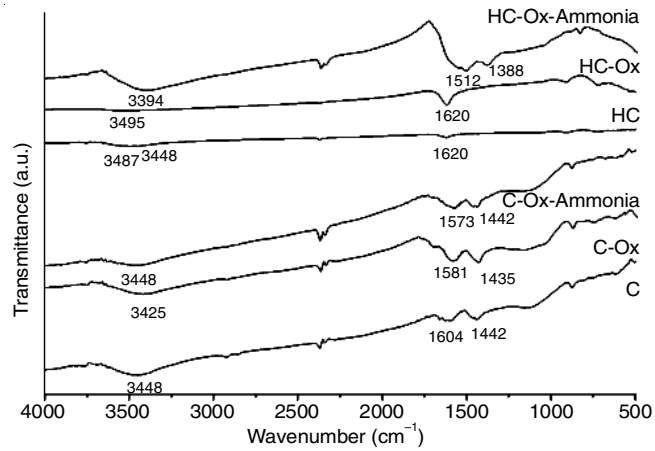

Fig. 4. FT-IR spectra of C, C-Ox, C-Ox-ammonia (after adsorbing NH_3), HC, HC-Ox and HC-Ox-ammonia (after adsorbing NH_3)

[26]. The NH_3 adsorbed mechanism on carbonized samples was the first, molecules gas of ammonia diffuse into the carbonized samples pore and was physically adsorbed at actives sites on the surface. The molecules of adsorbed NH_3 accept the proton to form ammonia complex ions (NH_4^+), so that act as the Brønsted acid from neighbor acidic groups [12].

Surface characteristics analysis: The analysis of the physical properties using nitrogen adsorption-desorption isotherm of samples prepared under hydrothermal and non-hydrothermal shown by Fig. 5a-b. The presence of mesopore confirmed by type IV isotherms with clear hysteresis type III (H3) for C-Ox and hysteresis type IV (H4) for HC-Ox. Type-H3 and H4 hysteresis loops in the relative pressure region between 0.15 and 1.0 showed the typical characteristic of mixed of microporous and mesoporous materials. Both of this type of hysteresis has been obtained with adsorbents having slit-shaped pores or plate-like particles (in the case of H3) [27], type-H3 occurs in very wide pores, but has a gap between parallel sheets [28], H4 is related to pores in the form of sheets but in micropores [29]. Table-1 showed C-Ox provided a higher BET surface area (443.5 m^2/g) than the HC-Ox sample (232.2 m^2/g). This was possible because the hydrothermal activation enhanced the formation of pores and further created new micropores, resulting in increasing of the total volume and decreasing of the diameter of the pore. However, when the carbonization process occurred, the sintering of the high-molecular-weight volatiles with the $ZnCl_2$ salt residue, resulting in the depolymerization of the melt of carbonized samples. The intermediate melt could seal off some of the pores in the carbon structure. Hydrothermal treatment would produce carbons with decreasing of the BET surface area and the diameter of pores, shown by pore distribution curves of these samples (Fig. 5c).

Morphology analysis using SEM: Figs. 6a-b depict the SEM images of the carbonized non-hydrothermal samples and hydrothermal (Fig. 6c-d) before and after the oxidizing process. All of them showed the overlapping tunnel, with a stacking honeycomb-like structure, indicating that the nature of the raw materials exert the influence on the morphologies of the carbon materials. The detailed structure due to the oxidation effect is further demonstrated by finer surface differences and cleaner tunnel formation. The differences in the shape and thickness of the wall are seen in the non-hydrothermal and hydrothermal samples. This might be related to the sintering of the high-molecular-weight volatiles with the $ZnCl_2$ salt residue was resulting in depolymerization at the carbonization process.

TABLE-1
ACIDITY AND CHARACTERISTICS OF POROSITY C-Ox and HC-Ox

Sample	Total acidity[a] (mmol/g)	S_{BET} (m^2/g)	V_{tot} (cm^3/g)	$D_{average}$ (nm)
C-Ox	3.376	443.5	0.01	5.437
HC-Ox	16.469	232.2	0.147	2.536

[a]Acidity of the catalyst was determined gravimetrically using adsorption NH_3 basic of gas.

Conclusion

The non-hydrothermal and hydrothermal treatment prepared the porous carbon materials from Merbau woods. The obtained carbonized have a high specific surface area with mesopores and showed a stacking honeycomb-like structure, indicating that the morphologies of the carbon materials mainly depend on the nature of the raw materials. The effect of hydrothermal treatment showed a decrease of specific surface area and the diameter of samples, because of the intermediate melt from depolymerization of the $ZnCl_2$ and the high-molecular-weight volatiles could seal off some of the pores in the carbon structure. Moreover, there was a change of shape and thickness of the wall structure of carbonized samples due to hydrothermal treatment.

ACKNOWLEDGEMENTS

The authors are grateful to the research grant from Ministry of Research, Technology and Higher Education, Republic of Indonesia under multiyears PDUPT 2019 (contract number: 2563/UN1.DITLIT/DIT-LIT/LT/2019).

CONFLICT OF INTEREST

The authors declare that there is no conflict of interests regarding the publication of this article.

REFERENCES

1. A.V. Chistyakov and M.V. Tsodikov, *Russ. J. Appl. Chem.*, **91**, 1090 (2018); https://doi.org/10.1134/S1070427218070054
2. D. Bergna, T. Varila, H. Romar and U. Lassi, *J. Carbon Res.*, **4**, 41 (2018); https://doi.org/10.3390/c4030041
3. M. Pongsendana, W. Trisunaryanti, F.W. Artanti, I.I. Falah and Sutarno, *Korean J. Chem. Eng.*, **34**, 2591 (2017); https://doi.org/10.1007/s11814-017-0165-3
4. L. Zhang, L. Jin, B. Liu and J. He, *Front. Chem.*, **7**, 22 (2019); https://doi.org/10.3389/fchem.2019.00022
5. W. Xin and Y. Song, RSC Adv., 5, 83239 (2015); https://doi.org/10.1039/C5RA16864C

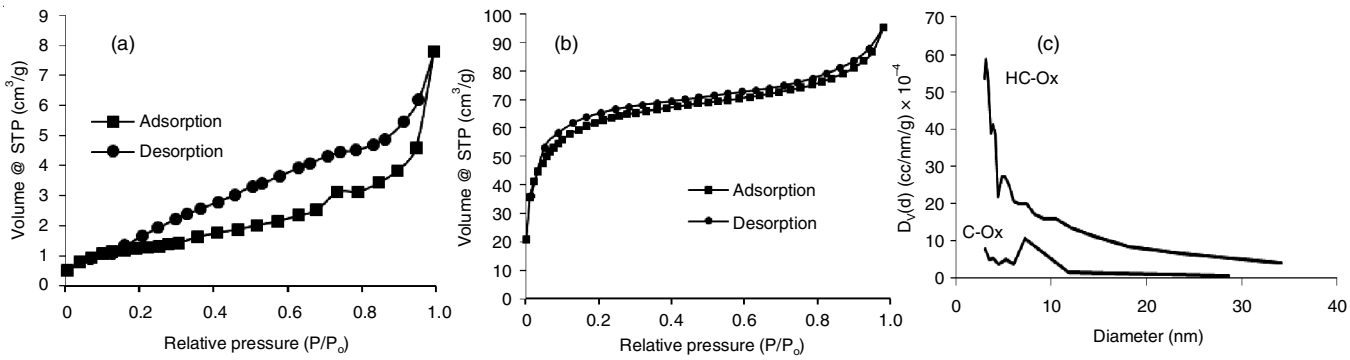

Fig. 5. Nitrogen adsorption-desorption isotherm of (a) C-Ox, (b) HC-Ox and (c) pore size distribution curves of C-Ox and HC-Ox

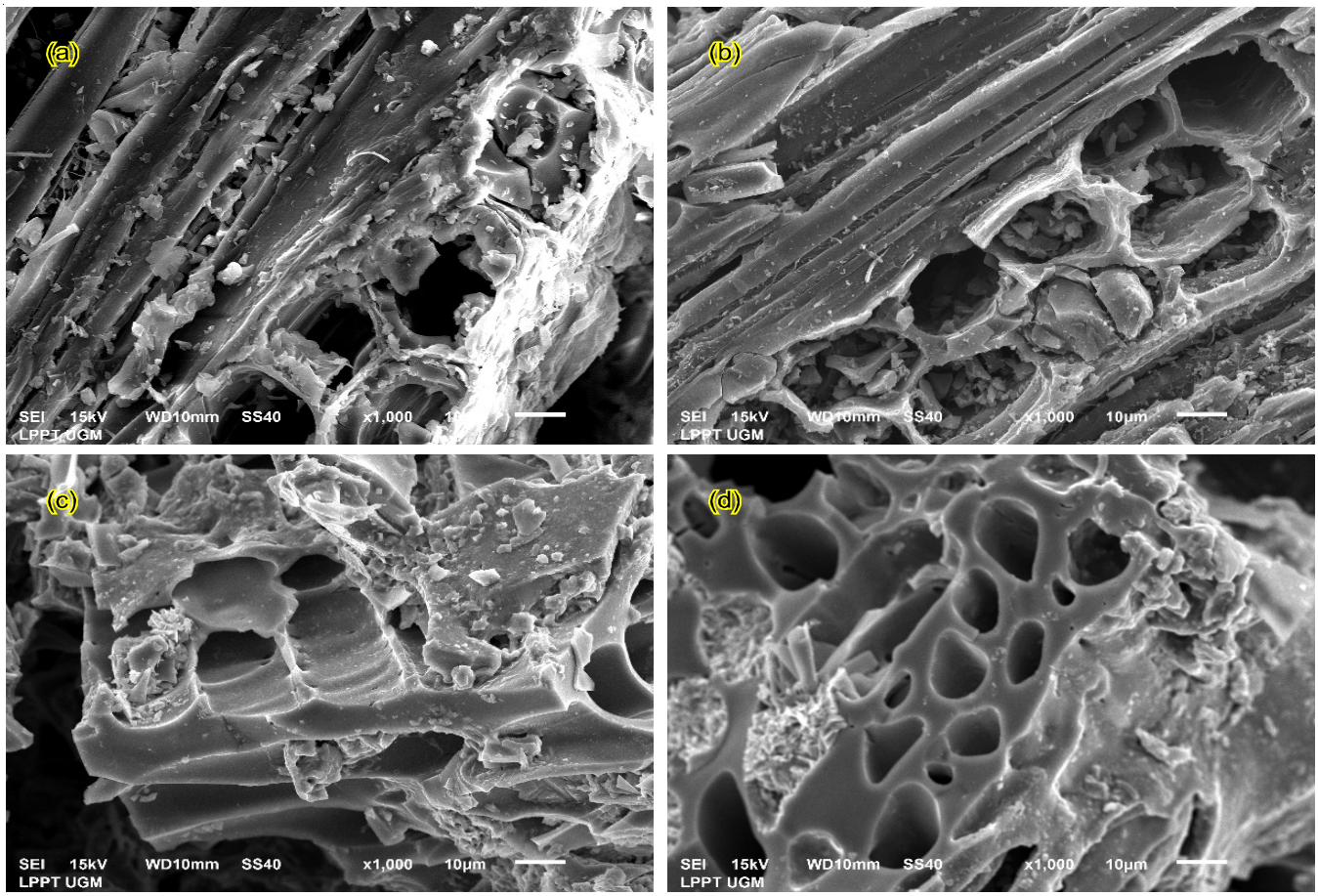

Fig. 6. SEM images of the (a) C, (b) C-Ox, (c) HC and (d) HC-Ox

6. J. Hayashi, N. Yamamoto, T. Horikawa, K. Muroyama and V.G. Gomes, *J. Colloid Interface Sci.*, **281**, 437 (2005); https://doi.org/10.1016/j.jcis.2004.08.092
7. Z. Hu and E.F. Vansant, *J. Colloid Interface Sci.*, **176**, 422 (1995); https://doi.org/10.1006/jcis.1995.9949
8. A. Jain, R. Balasubramanian and M.P. Srinivasan, *Chem. Eng. J.*, **273**, 622 (2015); https://doi.org/10.1016/j.cej.2015.03.111
9. A.D. Prasiwi, W. Trisunaryanti, Triyono, I.I. Falah, D. Santi, M.F. Marsuki, *Indones. J. Chem.*, **19**, 575 (2019). https://doi.org/10.22146/ijc.34189
10. A.V. Bridgwater and G.V.C. Peacocke, *Renew. Sustain. Energy Rev.*, **4**, 1 (2000); https://doi.org/10.1016/S1364-0321(99)00007-6
11. E. Apaydin-Varol and Y.A. Erulken, *J. Taiwan Inst. Chem. Eng.*, **54**, 37 (2015); https://doi.org/10.1016/j.jtice.2015.03.003
12. C.C. Huang, H.S. Li and C.H. Chen, *J. Hazard. Mater.*, **159**, 523 (2008); https://doi.org/10.1016/j.jhazmat.2008.02.051
13. L. Li, P.A. Quinlivan and D.R.U. Knappe, *Carbon*, **40**, 2085 (2002); https://doi.org/10.1016/S0008-6223(02)00069-6
14. S.L. Goertzen, K.D. Thériault, A.M. Oickle, A.C. Tarasuk and H.A. Andreas, *Carbon*, **48**, 1252 (2010); https://doi.org/10.1016/j.carbon.2009.11.050
15. P.T. Williams and S. Besler, *Renew. Energy*, **7**, 233 (1996); https://doi.org/10.1016/0960-1481(96)00006-7
16. A. Zeriouh and L. Belkbir, *Thermochim. Acta*, **258**, 243 (1995); https://doi.org/10.1016/0040-6031(94)02246-K
17. Y. Gao, Q. Yue, B. Gao, Y. Sun, W. Wang, Q. Li and Y. Wang, *Chem. Eng. J.*, **217**, 345 (2013); https://doi.org/10.1016/j.cej.2012.09.038
18. W. Li, K. Yang, J. Peng, L. Zhang, S. Guo and H. Xia, *Ind. Crops Prod.*, **28**, 190 (2008); https://doi.org/10.1016/j.indcrop.2008.02.012
19. M. Müller-Hagedorn, H. Bockhorn, L. Krebs and U. Müller, *J. Anal. Appl. Pyrolysis*, **68–69**, 231 (2003); https://doi.org/10.1016/S0165-2370(03)00065-2
20. A. Jain, S. Jayaraman, R. Balasubramanian and M.P. Srinivasan, *J. Mater. Chem. A Mater. Energy Sustain.*, **2**, 520 (2014); https://doi.org/10.1039/C3TA12648J
21. H. Shang, Y. Lu, F. Zhao, C. Chao, B. Zhang and H. Zhang, *RSC Adv.*, **5**, 75728 (2015); https://doi.org/10.1039/C5RA12406A
22. E. Altintig and S. Kirkil, *J. Taiwan Inst. Chem. Eng.*, **63**, 180 (2016); https://doi.org/10.1016/j.jtice.2016.02.032
23. S.H. Zeronian and M.K. Inglesby, *Cellulose*, **2**, 265 (1995); https://doi.org/10.1007/BF00811817
24. A.S. Amarasekara and C.C. Ebede, *Bioresour. Technol.*, **100**, 5301 (2009); https://doi.org/10.1016/j.biortech.2008.12.066
25. C. Kalinke, P.R. Oliveira, G. Oliveira, A.S. Mangrich, L.H. Marcolino-Junior and M.F. Bergamini, *Anal. Chim. Acta*, **983**, 103 (2017); https://doi.org/10.1016/j.aca.2017.06.025
26. L. Xie, Q. Gao, C. Wu and J. Hu, *Micropor. Mesopor. Mater.*, **86**, 323 (2005); https://doi.org/10.1016/j.micromeso.2005.07.044
27. S.J. Gregg and K.S.W. Sing, Adsorption, Surface Area and Porosity, Academic Press Inc.: London, edn 2 (1982).
28. K. Kaneko, *J. Membr. Sci.*, **96**, 59 (1994); https://doi.org/10.1016/0376-7388(94)00126-X
29. S. Lowell, J.E. Shields, M.A. Thomas and M. Thommes, Characterization of Porous Solids and Powders: Surface Area, Pore Size and Density. Choice Reviews Online, Springer Science Business Media: New York (2004).